Cortical network models of impulse firing in the resting and active states predict cortical energetics

Maxwell R. Bennett[a,b,1], Les Farnell[b,c], William G. Gibson[b,c], and Jim Lagopoulos[a]

[a]Brain and Mind Research Institute, University of Sydney, Camperdown, NSW 2050, Australia; and [b]Centre for Mathematical Biology and [c]School of Mathematics and Statistics, University of Sydney, Sydney, NSW 2006, Australia

Edited* by Rodolfo R. Llinas, New York University School of Medicine, New York, NY, and approved February 24, 2015 (received for review June 19, 2014)

Measurements of the cortical metabolic rate of glucose oxidation [$CMR_{glc(ox)}$] have provided a number of interesting and, in some cases, surprising observations. One is the decline in $CMR_{glc(ox)}$ during anesthesia and non-rapid eye movement (NREM) sleep, and another, the inverse relationship between the resting-state $CMR_{glc(ox)}$ and the transient following input from the thalamus. The recent establishment of a quantitative relationship between synaptic and action potential activity on the one hand and $CMR_{glc(ox)}$ on the other allows neural network models of such activity to probe for possible mechanistic explanations of these phenomena. We have carried out such investigations using cortical models consisting of networks of modules with excitatory and inhibitory neurons, each receiving excitatory inputs from outside the network in addition to intermodular connections. Modules may be taken as regions of cortical interest, the inputs from outside the network as arising from the thalamus, and the intermodular connections as long associational fibers. The model shows that the impulse frequency of different modules can differ from each other by less than 10%, consistent with the relatively uniform $CMR_{glc(ox)}$ observed across different regions of cortex. The model also shows that, if correlations of the average impulse rate between different modules decreases, there is a concomitant decrease in the average impulse rate in the modules, consistent with the observed drop in $CMR_{glc(ox)}$ in NREM sleep and under anesthesia. The model also explains why a transient thalamic input to sensory cortex gives rise to responses with amplitudes inversely dependent on the resting-state frequency, and therefore resting-state $CMR_{glc(ox)}$.

cortical networks | resting-state networks | impulse firing | cortical energetic

Classical measures of cortical activity, using cortical metabolic rate of glucose oxidation [$CMR_{glc(ox)}$], give results that are yet to be related in a mechanistic way with the underlying cortical excitability. There is a strict quantitative relationship between impulse and synaptic potential activity and $CMR_{glc(ox)}$ necessary to maintain this activity (1). The recent establishment of this relationship allows for an inquiry into how cortical excitability might give rise to observed changes in $CMR_{glc(ox)}$ in a number of different physiological conditions.

Variation in impulse activity between modules in some networks would be expected to reflect the observed variation in $CMR_{glc(ox)}$. Maximal reported differences of about 32% have been reported between different regions of cortex (2–4), but most cortical regions show much lower variations than this (3). The differences that do exist are not due to variations in thickness of cortex under consideration, nor to differences in the density of neurons (3). However, the differences may reflect that differences in the extent of cortico-cortical associational fiber connections for these are highest in posterior medial and parietal cortex (5), which have a relatively high oxidative demand (CMR_{O2}) and $CMR_{glc(ox)}$ in the brain (see supplementary figure 5 in ref. 3). The question then arises as to whether it is possible that a quantitative relationship exists between the level of action potential and synaptic activity in a cortical area and the extent to which this area receives associational fiber connections.

Correlations of signals between brain areas of subjects in the resting state have been taken to characterize resting-state functional networks (6), with the correlations probably mediated in many cases by synapses formed by associational fiber axons (7, 8). During sleep and anesthesia, some of these correlations are lost, indicating changes in synaptic transmission mediated by these fibers (9, 10). As there is concomitantly a significant decrease in $CMR_{glc(ox)}$ and hence the average impulse frequency in these areas (1), the question arises as to whether the decrease in $CMR_{glc(ox)}$ is due to a loss in average impulse frequency contingent on the loss of correlations. The cortical model presented here shows quantitatively that this is the case.

If the average resting-state CMR_{O2} is altered using anesthetics, then the changes in CMR_{O2} (ΔCMR_{O2}) following forepaw stimulation in the rat are significantly smaller the higher the average resting-state CMR_{O2} before stimulation (11, 12). Similar relationships are observed if impulse firing is measured rather than CMR_{O2} (11, 12). Also, the ΔCMR_{O2} spreads over a much larger area of cortex during the higher resting-state CMR_{O2}. Thus, for higher resting-state CMR_{O2}, the ΔCMR_{O2} spreads over S1 and S2 somatosensory cortex and M1 and M2 motor regions as well as some lateral regions of the hippocampus and some secondary areas of the visual and auditory cortex. In contrast, at lower resting-state CMR_{O2}, when ΔCMR_{O2} is comparatively large, it remains localized to the contralateral S1 and to an extent in S2 and M1 with no significant activation elsewhere (ref. 11; see also ref. 13). Even in awake primates, finger pad stimulation gives rise to a greater cortical spread of activation compared with anesthetized animals (14). Larger evoked signals are also recorded from cats and human visual cortex, with a clear quantitative inverse dependence of ΔCMR_{O2} to a visual stimulus on the average resting-state CMR_{O2} in this cortex: a 50% change in resting-state CMR_{O2} gives a 60% change in ΔCMR_{O2} (15). In addition, humans show both ΔCMR_{O2} and change in cerebral

Significance

Cortical metabolic rate of glucose oxidation [$CMR_{glc(ox)}$] measurements have provided quantitative estimates of cortical energetics associated with a number of physiological states, such as those that occur during sleep or under anesthesia. Recently, a strict quantitative relationship has been established between synaptic and action potential activity in a region of cortex and such measurements of $CMR_{glc(ox)}$, allowing neural networks to be used to probe the mechanistic basis of the $CMR_{glc(ox)}$ observations. Here, we use models of brain networks to provide such insights.

Author contributions: M.R.B. designed research; M.R.B., L.F., W.G.G., and J.L. performed research; M.R.B., L.F., and W.G.G. contributed new reagents/analytic tools; M.R.B., L.F., and J.L. analyzed data; and M.R.B., W.G.G., and J.L. wrote the paper.

The authors declare no conflict of interest.

*This Direct Submission article had a prearranged editor.

[1]To whom correspondence should be addressed. Email: max.bennett@sydney.edu.au.

This article contains supporting information online at www.pnas.org/lookup/suppl/doi:10.1073/pnas.1411513112/-/DCSupplemental.

www.pnas.org/cgi/doi/10.1073/pnas.1411513112

blood flow, in response to a visual signal, that are inversely dependent on average resting-state values (16). As an inverse relationship of evoked impulse firing on resting-state firing is reproduced in our cortical model, it provides an opportunity to seek out a plausible mechanistic basis of how it arises.

Although recent models of resting-state brain activity have used large-scale networks of cortico-cortical anatomical connectivity to analyze resting-state cortical activity (17–20), it is very useful to explore phenomenological models of lower complexity, for they allow insights concerning the important mechanisms that are active in the generation and dynamics of cortical activity (21). We have used such models, described in *Materials and Methods* and illustrated in Fig. 1, to provide plausible answers to the questions raised above concerning the relationships between $CMR_{glc(ox)}$ and cortical impulse activity.

Results

Cortical Networks. We have studied impulse activity in a number of networks, each consisting of different numbers of modules, with these containing a hundred neurons, 75% excitatory and 25% inhibitory, having different extents of synaptic connections both within and in the associational synaptic connections between modules (for details of this connectivity, see *Materials and Methods*, *Cortical Models*). The neurons within any module also receive synaptic connections external to the network representing, for instance, the intralaminar thalamic input. In addition, another input to the network may make synaptic connections in relation to the synapses formed by the intermodular associational connections whose efficacy they modify, as well as making synapses on neurons within modules of the network; this module may then represent, for instance, the basal nucleus. To simplify this network for computational purposes, the inputs external to the networks have been grouped and the control of the synaptic efficacy of the intermodular associational connections changed according to requirements rather than arising from the intrinsic workings of the basal nucleus/thalamus module in Fig. 1*A*. The projections within these modular networks are illustrated here by two networks with different levels of intermodular connectivity, designated network I (NI) and network II (NII), given in Fig. 1 *B* and *C*, respectively, from which the external modules have been removed for clarity. NI consists of eight modules (one in isolation for comparison with the rest), with each of these receiving between a single associational input from another module (modules 2 and 8), or inputs from two to three modules (module 6), with most (63%) of these inputs synapsing on excitatory neurons within modules, the rest on inhibitory neurons (Fig. 1*B*). In contrast to NI, NII (Fig. 1*C*) consists of seven modules, all of which receive two to eight associational synapses onto excitatory neurons and from zero to two associational synapses onto inhibitory neurons. NI and NII have been chosen from a large number of modular networks we have investigated, as they best illustrate principles that emerge from a study of small networks.

Associational Synaptic Connectivity and the Resting-State Impulse Frequency. The variation in the extent of $CMR_{glc(ox)}$, for networks NI and NII, in different regions of the cortex, due to differences in the resting-state impulse activity among the regions, is reflected in Fig. 2*A*. The impulse frequency in each of the modules in NI and NII in the resting state, that is when there is no enhanced transient input from the thalamic module to a specific network module (see below), can vary over threefold between modules, depending on their associational synaptic connections. For instance, in NI, modules 3, 4, and 6 each receive at least one associational input onto excitatory neurons, and one onto inhibitory neurons (Fig. 1*B*) and fire above the frequency of 18 Hz, averaged over all neurons in all modules. In contrast, modules 2 and 7 each receive an associational input that synapses only on an inhibitory neuron (Fig. 1*B*) and so maintain a relatively low average resting-state frequency of 8 Hz (Fig. 2*A*), much the same as module 1, which lacks any associational inputs (Figs. 1*B* and 2*A*). Module 8 receives only a single associational input onto an excitatory neuron and therefore fires at an intermediate resting-state frequency of about 15 Hz on average. On the other hand, NII, shown in Fig. 1*C*, possesses modules all of which receive at least two associational synaptic connections onto excitatory neurons and most of the other modules two or more associated synaptic connections onto inhibitory neurons. Because of this pattern of associational connectivity, the individual modules do not vary greatly in their resting-state frequency, only over a range from about 12 to 19 Hz on average (Fig. 2*A*). On the other hand, a much more uniform resting-state frequency can be engineered if the modules receive precisely the same number of associational connections. Fig. 2*B* shows that increasing the extent and uniformity of excitatory connections between modules increases the uniformity of impulse frequency in the modules. The network considered here consisted of excitatory connections between seven modules with each pair of modules possessing three efferent and three afferent excitatory connections (that is, three excitatory-to-excitatory connections in each direction between adjacent pairs of modules, making 42 in all). In this case, the mean frequency of impulses in each of the modules averages 20.0 ± 1.6, so the SD is only 8% of

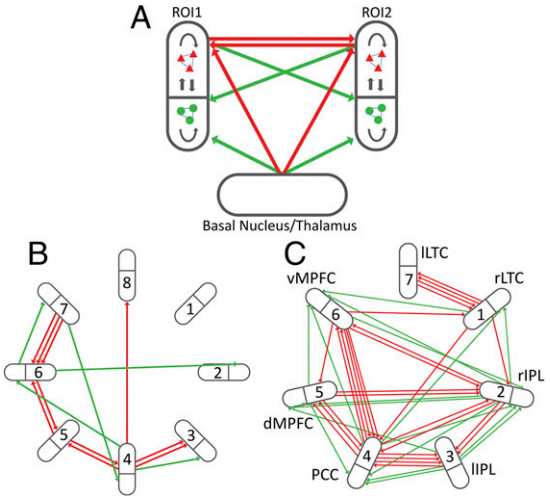

Fig. 1. Cortical network. (*A*) The basic model used in the present work. Shown are two modules (regions of interest, ROI_1 and ROI_2), represented by ellipses containing pools of excitatory neurons (red triangles) and inhibitory neurons (green circles), synaptically connected within and between pools (black arrows). The associational axons between ROI_1 and ROI_2 originate and end on single neurons and are either excitatory to excitatory (red arrows) or excitatory to inhibitory (green arrows). The input from the basal nucleus and thalamus is also excitatory; computationally, this input is represented by a Poisson train of impulses, the strength and frequency of which can be varied. (*B*) Intermodular connections in an eight-modular network (NI). The bold line within each module indicates separation of excitatory and inhibitory neurons within the module with all associational fibers between the modules forming excitatory synapses, primarily on excitatory neurons within the modules but not exclusively so. (*C*) Intermodular connections in a seven-modular network (NII). The connectivity due to the associational axons follows the criteria described in *A* above. NII may be taken to represent the default-mode network (DMN). In this case, the modules may be identified as follows: 1, rLTC; 2, rIPL; 3, lIPL; 4, PCC; 5, dMPFC; 6, vMPFC; 7, lLTC. The number and diversity of the associational fibers were chosen so as to reflect the reported weight of such connections between the modules of the DMN (see ref. 50, their figure 8 and associated table; also figure 4 *A* and 4*C* in ref. 51). Abbreviations are as follows: dMPFC and vMPFC, dorsal and ventral medial prefrontal cortex, respectively; PCC, posterior cingulate cortex; rIPL and lIPL, right and left inferior parietal lobe, respectively; and rLTC and lLTC, right and left lateral temporal cortex, respectively (from figure 8 in ref. 50).

NEUROSCIENCE

the mean (Fig. 2*B*). It should be noted that the frequency decreases or increases with a decrease or increase in the Poisson input to all of the modules (Fig. S1*C*). These networks illustrate that it is not the density of associational connections that determine the impulse frequency of modules, and hence their $CMR_{glc(ox)}$, but the pattern of the excitatory and inhibitory associational synaptic connections.

Loss of Correlated Impulse Firing Between Modules Accompanies Loss of Impulse Firing Within Modules. Correlated activity between regions of cortex can be modeled by networks such as NI and NII (Fig. 1 *B* and *C*). The NII can be used to model the default-mode network (DMN) (22) correlations both in awake and the changes that occur in non-rapid eye movement (NREM) sleep (for details of how the changes in correlations were carried out, see *SI Results* and Fig. S2). The loss of correlated activity between certain regions of the cortex in sleep and anesthesia is accompanied by $CMR_{glc(ox)}$ decreases of about 40% in these regions (1). The question arises as to what the relation is between the loss of correlations between regions, and that of impulse activity in these regions. In NII (the DMN), the average impulse firing drops in the modules as correlations are lost, as shown in Fig. 3. The decrease of the impulse rate in each of the seven modules of Fig. 1*C* is plotted in Fig. 3*A*. This shows an early decline as modules 1 and 7 are separated from modules 2–6 (with 1 and 7 either still connected or split from each other), and then an additional decline as modules 2–4 are separated from modules 5 and 6 (either with 1 and 7 still connected or split from each other). Fig. 3*B* shows the percentage decline of the average impulse frequency in each of the modules in these circumstances. The average decline across all modules is 38%, giving an expected decline in $CMR_{glc(ox)}$ of 38%, close to that of the observed experimental value of 40%. If, on the other hand, all of the correlations between the modules are gradually and uniformly decreased, then there is a gradual decrease in the average impulse frequency in each module, and hence in $CMR_{glc(ox)}$, until on average they decline about 50% (Fig. S3). However, none of these considerations take into account the possible loss of activity in the modules due to the decrease in their direct Poisson input with sleep and anesthesia, independent of a loss of correlated activity (for further discussion, see *SI Results* and Fig. S1*C*).

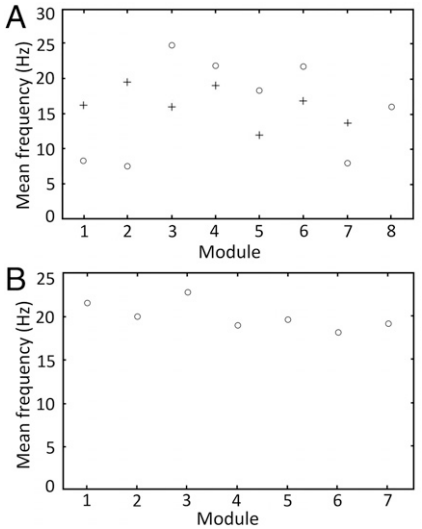

Fig. 2. (*A*) Mean frequency of impulses in the resting state within each module (1–8) for NI (circles) and the NII (crosses). (*B*) Mean frequency of impulses in the resting state within each module of a seven-module network in which there is uniform excitatory connections between the modules.

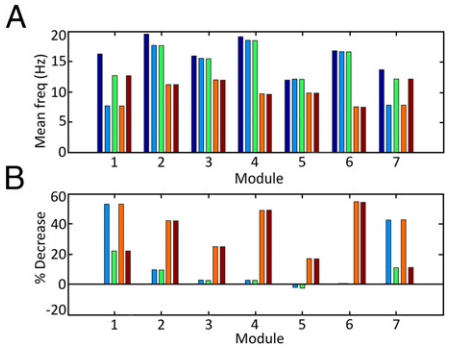

Fig. 3. (*A*) Changes in the impulse frequency in each of the seven modules of NII and (*B*) the percentage decrease in this frequency with progressive loss of correlated activity between the modules. This was effected by first isolating modules 1 and 7 [taken as the default-mode network (DMN) (lLTC and rLTC) from the network of modules 2–6 (rIPL, lIPL, PCC, dMPFC, vMPFC; Fig. S2] providing the first decline in frequency in all modules (dark blue, intact network; blue, split 1 and 7 from rest of the network and from each other; green, split 1 and 7 from network but leave them connected). Then modules 2–4 were isolated from modules 5–6, giving the final decline in frequency (orange, split 2 and 4 from 5 and 6 with 1 and 7 split; brown, split 2–4 from 5 and 6, with 1 and 7 still connected). Note in *B* that this last decline in correlation reduces the average frequency of impulses by 37 ± 14% in modules 2–4 and 33 ± 9% in modules 5–6 with an average overall decrease in impulse frequency over all modules of 38 ± 11%. Abbreviations are defined in the legend to Fig. 1*C*.

Short Transient Periods of Increased Impulse Firing in a Module, Due to Input from Outside the Network, Give Rise to Enhanced Rates of Firing Dependent on the Rate of the Resting-State Impulse Frequency. It has been repeatedly emphasized that the enhanced impulse frequency in a sensory cortical area, due to a specific increase in thalamic input, is increased if the resting-state background firing in the module is decreased by, for example, a general anesthetic (for a review, see ref. 23). We sought to examine the possible origins of this phenomenon in NI, which possesses modules with large differences in their resting-state frequencies. In particular, what is the possible mechanism responsible for the inverse relationship between the amplitude of the enhanced impulse frequency in a sensory cortical area due to a transient increase in thalamic input and the extent of the resting-state impulse activity? To examine this, we first showed that graded increases in the average frequency of the Poisson input to modules gave graded increases in the average firing rate in the module, whether the module was isolated or part of a network (Fig. 4 *A* and *B*). Next, the effect of 20-s transient increases in the Poisson input to an isolated module was determined. Finally, the effects of 20-s transient increases in the Poisson input to modules integrated in a network were determined. This showed that the transient increase in frequency elicited in a particular module was inversely proportional to the resting-state frequency of the module, with a gradient of −0.45 (Fig. 4*B*). This is similar to the experimental observations showing an inverse relationship between $\Delta CMR_{glc(ox)}$ in response to a thalamic input in either visual or somatosensory cortex and the resting-state baseline $CMR_{glc(ox)}$ (Fig. 4*D*) (11, 15). The regression line relating these had a gradient of −0.6, similar to the value above. [It might be noted that the same experimental gradient exists if the increase in frequency and the resting-state frequency are measured directly (12) instead of $\Delta CMR_{glc(ox)}$ and $CMR_{glc(ox)}$.] The inverse relationship held even for relatively small transient thalamic inputs (Fig. 4*C*) and could be determined by the internal dynamics of firing in individual modules (*SI Results*).

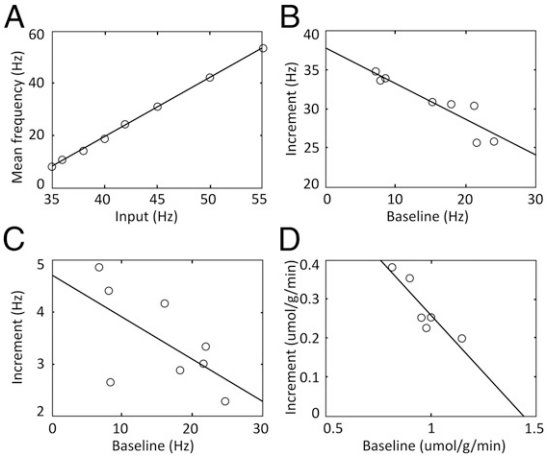

Fig. 4. (*A*) Impulse responses of an isolated module (no associational connections) to different frequencies of thalamic stimulation. There is a linear relation between the thalamic frequency of impulses to a module and the response of the module. (*B*) Increment in impulse frequency of each module in NI with all associational connections present, when the thalamic input frequency increases by the same relatively large amount to that module only. The results for each of the eight modules in NI are given, for which the resting-state base frequency varies as given in the abscissa from 8 to 24 Hz. Note that the increment in frequency of impulses in each module declines (from 35 to 26 Hz) with increase in the resting-state frequency of impulses in the module. The gradient of the regression line is −0.45. (*C*) Increment in impulse frequency of each module in NI (see Fig. 1*B* with all associational connections present, when the thalamic input frequency increases by the same relatively small amount to that module only). The results for each of the eight modules in the NI are given, for which the resting-state base frequency varies as given in the abscissa from 8 to 24 Hz. Note that the increment in frequency of impulses in each module declines (from 4.8 to 2.3 Hz) with the increase in the resting-state frequency of impulses in the module. The gradient of the regression line is −0.1. (*D*) Increment in $CMR_{glc(ox)}$ of visual cortex measured in cats following a visual stimulus when the cortex possesses different resting states. The regression line through the experimental points has a gradient of −0.6, similar to the theoretical gradient in *B* (15). A similar gradient relates incremental changes in impulse firing to baseline impulse firing in the rat somatosensory cortex following a tactile stimulus (11).

Discussion

Variations of Impulse Frequency over Modules and of $CMR_{glc(ox)}$ over Cortex. Resting-state functional networks are constrained by structural connections (24). Patterns of functional connectivity, that is patterns of correlations of neural activity, can share common structural motifs (25), with a network core and distribution of "cliques" (26). It has been claimed that network cores tend to have high levels of $CMR_{glc(ox)}$, suggesting that a causal relationship might exist between the regions of high associational synaptic connectivity, taken as network cores, and the average impulse activity. We found typically a variation of up to 30% in average impulse activity and therefore in $CMR_{glc(ox)}$ between modules in a network that received at least one excitatory associational fiber input, although for those that did not receive such an input the variation rose to threefold. Without further extensive investigation, it is not clear what the relative contributions are of the density of innervation of the modules on the one hand and the pattern of innervation distributed between excitation and inhibition on the other to the activity of the modules.

Correlated Impulse Fluctuations over Modules During Sleep. During NREM sleep, there is a fall in correlated activity between some areas constituting the DMN and an increase in others (27, 28). The greatest decline, of over 70%, occurs between the medial prefrontal cortex (MPFC) and the posterior cingulate cortex (PCC) and also between the MPFC and the right inferior parietal lobule (IPL); on the other hand, there is an increase of over 70% in the correlated activity between the PCC and the left IPL (see table 2 in ref. 29 and also ref. 30). In the present work, the DMN was modeled using NII, and in this case the modules representing the MPFC correlations with both the PCC and IPL module representations were forced to zero by disconnecting the appropriate associational fibers resulting in the correlations between PCC and left IPL increasing (Fig. S3), as is observed. This reflects the fact that NREM sleep is accompanied by fewer long-range effective associational connections with increased "cliqueness" of local connections (that is, there is a clustering of local "submodules") (27, 28, 31).

Loss of Average Resting-State Impulse Frequency over Modules During Sleep and Anesthesia. Given that during sleep many correlations are lost, indicating a fall of functional associational connectivity that has been argued is due to a loss of effective associational connections, then there should be a significant decrease in impulse activity in individual modules, accompanied by a decrease in $CMR_{glc(ox)}$ in these modules. This is observed for there is a global drop in $CMR_{glc(ox)}$ in NREM sleep compared with awake of 36%, with differences in different parts of the brain of 31–38%. The global drop in impulse activity was 38% for NII (taken to represent the DMN), varying between modules from 24% to 52%, when correlations between MPFC and both the PCC and IPL were forced to zero. The model predicts a 38% drop, similar to the observed drop of 36% in $CMR_{glc(ox)}$. It has been claimed, however, that "decoupling of frontal and parietal regions during deep sleep is not simply due to reduced frontal activity given that the amplitude of the fluctuations within that region remained unchanged" (table 4 in ref. 10). However, table 4 in ref. 10 shows reductions in the rms value of the fluctuations of 23% for MPFC and 10% for IPL with a rise of 32% in PCC, indicating that there are significant decreases in blood oxygen level-dependent fluctuations in some areas, presumably reflecting decreases in the SD of the impulse fluctuations in turn reflecting decreases in average impulse frequency and so in $CMR_{glc(ox)}$.

During quiet wakefulness, transcranial magnetic stimulation of the premotor area leads to an initial electrical response there, followed by a sequence of waves that propagate to other areas of the cortex with which the premotor area has long associational connections. This is in contrast to NREM sleep or anesthesia when the electrical response at the premotor site of stimulation is strong but does not propagate to other sites (29, 30), perhaps due to reduction in the effective connections of cortical areas/modules (32).

Propofol anesthesia similarly reduces functional connectivity (33, 34). For example, the functional connectivity of the MPFC is reduced in the DMN from 0.6 to 0.1 and that of the PCC from 0.6 to 0.3. These decreases are accompanied by decreases in $CMR_{glc(ox)}$ of about 50–60% in different areas of cortex (35), as expected from the relationship between decreases in impulse activity in different modules and their loss of functional connectivity (Fig. 3).

Relation Between Average Resting-State Impulse Frequency and Evoked Increases in Impulse Frequency. An inverse relationship exists between the amplitude of signals in a sensory area of cortex in response to a transient increase in thalamic input and that of the resting-state activity in that area, whether these are measured in terms of impulse activity or CMR_{O2} (11, 15, 16). It arises because of the additional impulse activity from the thalamus failing to give an increase in activity if this addition occurs during ongoing resting-state activity: if the latter increases, thus the former decreases (*SI Results*). It is notable that the same inverse relation does not occur if there is just an increase in

resting-state activity that arises from the intrinsic workings of the network, independent of any extra external inputs, such as those from the thalamus. Thus, observed changes, in at least sensory areas of cortex in response to transient inputs from the thalamus, must take account of the resting-state activity. However, changes that occur as a consequence of fluctuations in the intrinsic activity of the cortex, as used for example to determine functional connectivity through correlations, are unlikely to be subject to such a consideration.

Materials and Methods

Cortical Models. Networks have been modeled in a variety of ways. In some, cortical areas or modules are treated as nodes, each consisting of a network of synaptically coupled and interconnected excitatory and inhibitory neurons, with these nodes joined by associational synaptic connections. The mesoscopic dynamics of such networks have been examined when the activity of the nodes is generated using mean field equation approximations (36, 37); local dynamics in the nodes are then determined by voltage and ligand-gated ion channels as well as the recurrent feedback connections between the neurons (38). Others use Wilson–Cowan phase oscillating units for modules generating oscillations in the gamma range (30–80 Hz), with these modules then integrated into networks by means of intermodular connections.

We have used such networks in the present work. In these networks, the modules, representing cortical areas, consist of relatively large numbers of excitatory and inhibitory neurons (75% of the former and 25% of the latter, in agreement with observations of ref. 39) with recurrent synaptic connections. These synaptic connections were on average (±SD) as follows: excitatory to excitatory, 14.1 ± 3.6; excitatory to inhibitory, 14.6 ± 3.17; inhibitory to excitatory, 5.12 ± 2.10. The ratio of excitatory-to-inhibitory connections to the excitatory neurons was then 0.36. This ratio varies over excitatory pyramidal neurons from 0.10 on distal dendrites to 0.98 on the soma (40). The inhibitory connections on the soma are very powerful in determining impulse initiation and propagation from the soma, so we settled for an inhibitory-to-excitatory ratio of 0.36 on average. The strengths of the inhibitory and excitatory connections are given in Table S1, providing an excitatory-to-inhibitory ratio of strengths of 0.33. This may be compared with that reported in the literature of from 0.5 (41) to 1.0 (42). Again, we erred on the side of emphasizing the inhibitory strengths because of the powerful inhibitory effects at the soma.

The neurons in the network also receive an external background input of uncorrelated Poisson impulse trains, like those that cortical neurons receive from the basal nucleus and intralaminar nuclei of the thalamus, together with intermodular excitatory synaptic connections (compare with the network in ref. 18; see also ref. 7). In addition to the introduction of appropriate delays on the intermodular synaptic connections, these were taken as capable of modification by another source external to the modular network, one which may be identified with the cholinergic projections to the cortex from the basal nucleus of Meynert (7). It should be noted that, in networks that most closely resemble the above, such as that of ref. 18, there are also separate cholinergic inputs to the modules, but the principal actions of these inputs is to inhibit the release of glutamate from the intermodular synaptic connections and to reduce the impulse frequency adaptation in the neurons of the modules. As the DMN is at present the resting-state network (RSN) of greatest interest, particularly in the context of computational simulations (see, e.g., ref. 43), we have concentrated our analysis on this RSN in some aspects of the present work.

The patterns of impulse firing in the cortex are very irregular (44–46), with some showing bursts followed by relatively silent periods of about 0.5 s (47) as observed in the present simulations. The patterns of firing are determined by the intrinsic properties of modular networks and the nature of the input to the networks, which in the present case is a Poisson input to all of the neurons, excitatory and inhibitory, in the network. Thus, although not reported in detail here, other forms of input, such as a uniform distribution rather than a Poisson distribution, might give rise to different patterns of network firings. For the present purposes, this Poisson firing input to the networks and of the networks themselves is a condition on the relationships presented in *SI Results*.

The model uses networks of integrate-and-fire neurons. Fig. 1*A* depicts a system of two interconnected modules, each containing an identical neural network. This network contains pools of excitatory neurons (red triangles) and inhibitory neurons (green circles), synaptically connected within and between pools (black arrows). The long arrows indicate connections between the neurons in different modules, either excitatory to excitatory (red arrows) or excitatory to inhibitory (green arrows); the strength of these connections can be modified, for example by input from a basal nucleus or thalamus, as shown.

Single Module. We first give the formalism for the network in a single isolated module, following that of ref. 7, which in turn was based on refs. 48 and 49.

The membrane potential V of a single neuron is governed by the following:

$$\frac{dV}{dt} = -g_L(V - V_L) - g_E(t)(V - V_E) - g_I(t)(V - V_I), \quad [1]$$

where g_L is the leak conductance, and $g_E(t)$ and $g_I(t)$ are the time-dependent conductances arising from external inputs and from the network activity of excitatory and inhibitory neurons. These conductances have been normalized by the membrane potential and thus have the dimension of inverse time. V_L is the rest potential, and V_E and V_I are the excitatory and inhibitory reversal potentials, respectively.

The membrane potential of a neuron evolves according to integrate-and-fire dynamics. A spike is generated when $V = V_T$; V is then reset to $V_R (< V_T)$ and held there for an absolute refractory period τ_{ref}. The membrane potential is normalized so that $V_T = 1$ and $V_R = 0$.

The network contains N neurons, of which N_E are excitatory and N_I are inhibitory. The conductance change in a typical neuron due to excitatory inputs is as follows:

$$g_E(t) = g_E^0(t) + \sum_k A_k \sum_l G_E\left(t - t_l^k\right), \quad [2]$$

where g_E^0 is the contribution from external excitatory sources, A_k is the connection strength from the kth excitatory neuron, and $G_E(t - t_l^k)$ describes the effect of the postsynaptic current generated by an action potential in neuron k at time t_l^k. This function is taken to have an α-like form:

$$G_E(t) = \frac{1}{6\tau_E}\left(\frac{t}{\tau_E}\right)^3 exp\left(-\frac{t}{\tau_E}\right)\theta(t), \quad [3]$$

where $\theta(t) = 1$ for $t > 0$ and 0 otherwise; τ_E is the time constant for excitatory neurons.

The sum Σ_k is over all neurons connected to the excitatory neuron under consideration, and Σ_l is over all firings of neuron k up to time t. Similarly, the conductance change in a typical neuron due to inhibitory inputs is as follows:

$$g_I(t) = g_I^0(t) + \sum_k B_k \sum_l G_I\left(t - t_l^k\right), \quad [4]$$

where B_k is the connection strength from the kth inhibitory neuron and $G_I(t)$ is given by Eq. **3** with τ_E replaced by τ_I. The sums over k in Eqs. **2** and **4** are over all neural connections; in the computations, a fraction F of all N neurons are connected, with no distinction made between excitatory and inhibitory neurons.

The time evolution of the network is initiated by trains of independent but identically distributed Poisson inputs applied to each neuron. Parameters A_k, B_k, and F, as well as the rate and strength of the Poisson input, are chosen so that there is a low average firing rate (~8 Hz) of all of the neurons in the module.

System. The complete system consists of N_M identical modules that are interconnected by a limited number of synaptic connections originating from single excitatory neurons and ending on either excitatory or inhibitory neurons, both connected neurons being randomly selected from the appropriate pool. For NI, $N_M = 8$ and the intermodal connections were generated randomly (Fig. 1*B*), with the strength of each coupling given by the same parameter values A_k as for the intramodal couplings. The number of couplings was adjusted to obtain reasonable average firing rates for the whole system. For NII, $N_M = 7$ and the connections are based on physiological data (Fig. 1*C*); to achieve reasonable firing rates, the connection strengths were reduced to 45% of those in NI, with further decreases in the firing rates possible by decreasing the Poisson input to the modules (Fig. S1*C*). As stated in the legend to Fig. 1, "The number and diversity of the associational fibers were chosen so as to reflect the reported weight of such connections between the modules of the DMN (see ref. 50, their figure 8 and associated table; also figure 4 *A* and *C* in ref. 51)." Interestingly, this gives a maximum variation of the activity between modules (2, 5) of 30%, which we wanted to achieve given the maximum variation measured of 32% mentioned in the Introduction. In addition, it gives a relatively small variation over all modules of 16% (average ± SD of 16.4 ± 2.7 Hz), again approximating the goal of

having only relatively small variations over most of the cortex. We have also investigated networks with higher levels of connectivity and symmetry than that given by NII (Fig. 2*B*), and these show as expected even smaller variations in activity from module to module of 8% (average ± SD of 20.01 ± 1.6 Hz; Fig. 2*B*).

A time delay t_d was imposed on the transmission between modules. Simulation runs were generally of 300-s duration, using a time step of 0.01 ms and data sampling every 100 ms. In the cases where extra stimulation was applied to a module, this was turned on at 25 ms and then alternated 20 s on and 20 s off until the end of the run.

1. Hyder F, Rothman DL, Bennett MR (2013) Cortical energy demands of signaling and nonsignaling components in brain are conserved across mammalian species and activity levels. *Proc Natl Acad Sci USA* 110(9):3549–3554.
2. Buchsbaum MS, et al. (1989) Regional cerebral glucose metabolic rate in human sleep assessed by positron emission tomography. *Life Sci* 45(15):1349–1356.
3. Hyder F, Fulbright RK, Shulman RG, Rothman DL (2013) Glutamatergic function in the resting awake human brain is supported by uniformly high oxidative energy. *J Cereb Blood Flow Metab* 33(3):339–347.
4. Tomasi D, Wang GJ, Volkow ND (2013) Energetic cost of brain functional connectivity. *Proc Natl Acad Sci USA* 110(33):13642–13647.
5. Hagmann P, et al. (2008) Mapping the structural core of human cerebral cortex. *PLoS Biol* 6(7):e159.
6. Biswal BB, Van Kylen J, Hyde JS (1997) Simultaneous assessment of flow and BOLD signals in resting-state functional connectivity maps. *NMR Biomed* 10(4-5):165–170.
7. Bennett MR, Farnell L, Gibson WG (2013) Fiber pathway pathology, synapse loss and decline of cortical function in schizophrenia. *PLoS One* 8(4):e60518.
8. Bowman FD, Zhang L, Derado G, Chen S (2012) Determining functional connectivity using fMRI data with diffusion-based anatomical weighting. *Neuroimage* 62(3):1769–1779.
9. Guldenmund P, et al. (2013) Thalamus, brainstem and salience network connectivity changes during propofol-induced sedation and unconsciousness. *Brain Connect* 3(3):273–285.
10. Horovitz SG, et al. (2009) Decoupling of the brain's default mode network during deep sleep. *Proc Natl Acad Sci USA* 106(27):11376–11381.
11. Maandag NJ, et al. (2007) Energetics of neuronal signaling and fMRI activity. *Proc Natl Acad Sci USA* 104(51):20546–20551.
12. Smith AJ, et al. (2002) Cerebral energetics and spiking frequency: The neurophysiological basis of fMRI. *Proc Natl Acad Sci USA* 99(16):10765–10770.
13. Masamoto K, Kim T, Fukuda M, Wang P, Kim SG (2007) Relationship between neural, vascular, and BOLD signals in isoflurane-anesthetized rat somatosensory cortex. *Cereb Cortex* 17(4):942–950.
14. Chen LM, Friedman RM, Roe AW (2005) Optical imaging of SI topography in anesthetized and awake squirrel monkeys. *J Neurosci* 25(33):7648–7659.
15. Zhu XH, Zhang N, Zhang Y, Ugurbil K, Chen W (2009) New insights into central roles of cerebral oxygen metabolism in the resting and stimulus-evoked brain. *J Cereb Blood Flow Metab* 29(1):10–18.
16. Pasley BN, Inglis BA, Freeman RD (2007) Analysis of oxygen metabolism implies a neural origin for the negative BOLD response in human visual cortex. *Neuroimage* 36(2):269–276.
17. Cabral J, Hugues E, Sporns O, Deco G (2011) Role of local network oscillations in resting-state functional connectivity. *Neuroimage* 57(1):130–139.
18. Deco G, Hagmann P, Hudetz AG, Tononi G (2013) Modeling resting-state functional networks when the cortex falls sleep: Local and global changes. *Cereb Cortex* 24(12):3180–3194.
19. Honey CJ, et al. (2009) Predicting human resting-state functional connectivity from structural connectivity. *Proc Natl Acad Sci USA* 106(6):2035–2040.
20. Zuo XN, et al. (2012) Network centrality in the human functional connectome. *Cereb Cortex* 22(8):1862–1875.
21. Ritter P, Schirner M, McIntosh AR, Jirsa VK (2013) The virtual brain integrates computational modeling and multimodal neuroimaging. *Brain Connect* 3(2):121–145.
22. Raichle ME, et al. (2001) A default mode of brain function. *Proc Natl Acad Sci USA* 98(2):676–682.
23. Shulman RG, Rothman DL, Hyder F (2007) A BOLD search for baseline. *Neuroimage* 36(2):277–281.
24. Park HJ, Friston K (2013) Structural and functional brain networks: From connections to cognition. *Science* 342(6158):1238411.
25. Sporns O, Tononi G, Edelman GM (2002) Theoretical neuroanatomy and the connectivity of the cerebral cortex. *Behav Brain Res* 135(1-2):69–74.
26. Ercsey-Ravasz M, et al. (2013) A predictive network model of cerebral cortical connectivity based on a distance rule. *Neuron* 80(1):184–197.
27. Boly M, et al. (2012) Hierarchical clustering of brain activity during human nonrapid eye movement sleep. *Proc Natl Acad Sci USA* 109(15):5856–5861.
28. Spoormaker VI, Gleiser PM, Czisch M (2012) Frontoparietal connectivity and hierarchical structure of the brain's functional network during sleep. *Front Neurol* 3:80.
29. Massimini M, et al. (2007) Triggering sleep slow waves by transcranial magnetic stimulation. *Proc Natl Acad Sci USA* 104(20):8496–8501.
30. Massimini M, et al. (2005) Breakdown of cortical effective connectivity during sleep. *Science* 309(5744):2228–2232.
31. Spoormaker VI, et al. (2010) Development of a large-scale functional brain network during human non-rapid eye movement sleep. *J Neurosci* 30(34):11379–11387.
32. Ferrarelli F, et al. (2010) Breakdown in cortical effective connectivity during midazolam-induced loss of consciousness. *Proc Natl Acad Sci USA* 107(6):2681–2686.
33. Boveroux P, et al. (2010) Breakdown of within- and between-network resting state functional magnetic resonance imaging connectivity during propofol-induced loss of consciousness. *Anesthesiology* 113(5):1038–1053.
34. Fiset P, et al. (1999) Brain mechanisms of propofol-induced loss of consciousness in humans: A positron emission tomographic study. *J Neurosci* 19(13):5506–5513.
35. Schlünzen L, Juul N, Hansen KV, Cold GE (2012) Regional cerebral blood flow and glucose metabolism during propofol anaesthesia in healthy subjects studied with positron emission tomography. *Acta Anaesthesiol Scand* 56(2):248–255.
36. Jirsa VK, Stefanescu RA (2011) Neural population modes capture biologically realistic large scale network dynamics. *Bull Math Biol* 73(2):325–343.
37. Stefanescu RA, Jirsa VK (2011) Reduced representations of heterogeneous mixed neural networks with synaptic coupling. *Phys Rev E Stat Nonlin Soft Matter Phys* 83(2 Pt 2):026204.
38. Breakspear M, Terry JR, Friston KJ (2003) Modulation of excitatory synaptic coupling facilitates synchronization and complex dynamics in a biophysical model of neuronal dynamics. *Network* 14(4):703–732.
39. Fitzpatrick D, Lund JS, Schmechel DE, Towles AC (1987) Distribution of GABAergic neurons and axon terminals in the macaque striate cortex. *J Comp Neurol* 264(1):73–91.
40. Megías M, Emri Z, Freund TF, Gulyás AI (2001) Total number and distribution of inhibitory and excitatory synapses on hippocampal CA1 pyramidal cells. *Neuroscience* 102(3):527–540.
41. Thomson AM, West DC, Wang Y, Bannister AP (2002) Synaptic connections and small circuits involving excitatory and inhibitory neurons in layers 2-5 of adult rat and cat neocortex: Triple intracellular recordings and biocytin labelling in vitro. *Cereb Cortex* 12(9):936–953.
42. Dantzker JL, Callaway EM (2000) Laminar sources of synaptic input to cortical inhibitory interneurons and pyramidal neurons. *Nat Neurosci* 3(7):701–707.
43. Senden M, Goebel R, Deco G (2012) Structural connectivity allows for multi-threading during rest: The structure of the cortex leads to efficient alternation between resting state exploratory behavior and default mode processing. *Neuroimage* 60(4):2274–2284.
44. Connors BW, Gutnick MJ (1990) Intrinsic firing patterns of diverse neocortical neurons. *Trends Neurosci* 13(3):99–104.
45. Gray CM, McCormick DA (1996) Chattering cells: Superficial pyramidal neurons contributing to the generation of synchronous oscillations in the visual cortex. *Science* 274(5284):109–113.
46. Softky WR, Koch C (1993) The highly irregular firing of cortical cells is inconsistent with temporal integration of random EPSPs. *J Neurosci* 13(1):334–350.
47. Ranck JB, Jr (1973) Studies on single neurons in dorsal hippocampal formation and septum in unrestrained rats. I. Behavioral correlates and firing repertoires. *Exp Neurol* 41(2):461–531.
48. Tao L, Shelley M, McLaughlin D, Shapley R (2004) An egalitarian network model for the emergence of simple and complex cells in visual cortex. *Proc Natl Acad Sci USA* 101(1):366–371.
49. Tao L, Cai D, McLaughlin DW, Shelley MJ, Shapley R (2006) Orientation selectivity in visual cortex by fluctuation-controlled criticality. *Proc Natl Acad Sci USA* 103(34):12911–12916.
50. Buckner RL, Andrews-Hanna JR, Schacter DL (2008) The brain's default network: Anatomy, function, and relevance to disease. *Ann N Y Acad Sci* 1124:1–38.
51. Eldaief MC, Halko MA, Buckner RL, Pascual-Leone A (2011) Transcranial magnetic stimulation modulates the brain's intrinsic activity in a frequency-dependent manner. *Proc Natl Acad Sci USA* 108(52):21229–21234.